



ORIGINAL ARTICLE

Numerical analysis of composite steel and concrete beams subjected to fire under different support conditions

Análise numérica de vigas mistas de aço e concreto em situação de incêndio sob diferentes condições de apoios

Lucas Coscia Romagnoli^a Valdir Pignatta e Silva^a ^aUniversidade de São Paulo – USP, Escola Politécnica, Departamento de Engenharia de Estruturas e Geotécnica, São Paulo, SP, Brasil

Received 16 October 2019

Accepted 26 February 2020

Abstract: To evaluate the behavior of semi-continuous composite beams in fire, six finite elements numerical models with several steel profiles and slab dimensions were developed in ABAQUS software. The models took into account several behaviors usually suppressed in simplified analyzes such as: geometric and materials non-linearity properties and thermal expansion effects, including indirect stresses. Three support conditions were analyzed: simply supported (axial released), axial restrained and semi-continuous, totaling 18 analyzes. The different support conditions results were compared to each other and to the fire resistance time designed by simplified methods, which followed design code recommendations.

Keywords: fire, composite steel concrete beam, semi-continuous, numerical analysis.

Resumo: Com o objetivo de avaliar o comportamento de vigas mistas semicontínuas em situação de incêndio considerando diversos fenômenos desprezados em análises simplificadas como não linearidade geométrica, não linearidade das propriedades térmicas e mecânicas dos materiais e efeitos da dilatação térmica, incluindo esforços solicitantes indiretos, foram desenvolvidos seis modelos numéricos em elementos finitos no programa de computador ABAQUS com geometrias distintas, alterando as dimensões do perfil de aço e laje que compõe a viga mista. Para cada um dos seis modelos foram analisadas três condições de contorno, sendo elas: simplesmente apoiada (livre axialmente), biapoiada (restringida axialmente) e semicontínua, totalizando 18 análises. Os resultados das diferentes condições de contorno foram comparados entre si, além do TRF do caso semicontínuo encontrado por método simplificado, que seguiu recomendações normatizadas.

Palavras-chave: incêndio, viga mista de aço e concreto, semicontínua, análise numérica.

How to cite: L. C. Romagnoli and V. P. Silva, “Numerical analysis of composite steel and concrete beams subjected to fire under different support conditions,” *Rev. IBRACON Estrut. Mater.*, vol. 13, no. 5, e13513, 2020, <https://doi.org/10.1590/S1983-41952020000500013>

1 INTRODUCTION

1.1 Objective

A composite steel and concrete beam designed at room temperature usually does not offer adequate structural safety when checked for fire according to design codes, unless fireproof is provided. Such solution leads to higher costs that, at a national level, often make the choice for structural steel systems impracticable.

This study goal is to assess the behavior of composite steel and concrete beams in fire taking in consideration the rotational stiffness of the supports provided by the slab’s mesh reinforcement and the restriction of the profile’s lower flange, creating a composite connection, as shown in Figure 1, and ensuring a semi-continuous behavior to the beam.

Corresponding author: Lucas Coscia Romagnoli. E-mail: lucas.romagnoli@usp.br

Financial support: Grant 2018/14735-6, São Paulo Research Foundation (FAPESP) and Conselho Nacional de Pesquisa e Desenvolvimento Científico (CNPq).

Conflict of interest: Nothing to declare.



This is an Open Access article distributed under the terms of the Creative Commons Attribution License, which permits unrestricted use, distribution, and reproduction in any medium, provided the original work is properly cited.

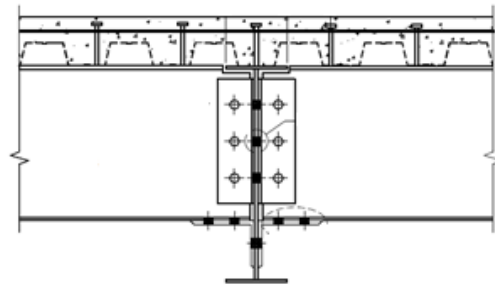


Figure 1. Composite connection (Source: adapted from ABNT NBR 8800 [1]).

The semi-continuous solution is able to increase significantly the beam's bending load strength at room temperature. The studies aim to quantify the fire resistance time increase provided by this solution, evaluating the hypothesis of not relying on fireproof coating for cases in which such increase is shown to be sufficient.

However, when a steel beam is under and in contact with a concrete slab, one of its faces is not exposed to fire, since the slab provides protection to the profile's upper flange, leading to a non-uniform internal temperature distribution. This thermal gradient along the cross-section causes additional deformations and indirect stresses due to supports rotational restraints. If the structure is already subject to negative bending moments at the supports, as in the case of a semi-continuous beam, these may be amplified during fire exposure.

This harmful effect was evaluated with aid of nonlinear thermo-structural numerical analysis, exposed in this paper. The numerical models considered effects such as catenary stresses on the slab, resulted from large deformations, and material nonlinear behavior. Both those effects reduces the thermal expansion indirect stresses.

Previous results [2] showed that for semi-continuous composite beams the bending moment capacity increase, compared to the simply supported case, is enough to dispense fireproof coating for standard-fire resistance requirements of less than 30 min. These calculations followed design code procedures that consider the formation of plastic hinges on the supports and mid-span as the ultimate limit state.

These previous studies accounted for simplifying hypotheses, which neglected indirect stresses caused by thermal expansion and thermal gradient. An attempt to propose a method of increasing stresses without considering other complex behaviors such as materials nonlinearity and large deformations would excessively penalize the simplified model, leading to very conservative results (as already evidenced by Silva [3] in case of indirect stresses in axial restrained steel beams and simple frames subjected to temperatures close to critical).

It is important to note that although IT 8 [4] tabular method indicates a minimum standard-fire resistance time of 30 min, it is possible to adopt lower times for small buildings with low fire load by utilizing the equivalent time method. This method is detailed in ABNT NBR 15200 [5], ABNT NBR 14323 [6] and IT 8 [4], and commented by Silva et al. [7].

This present paper analyzed the simplifying hypotheses adopted in Romagnoli and Silva [2]. Additional information is described in detail in Romagnoli [8].

1.2 Background

Usually the choice for steel structures is associated with the essential need of adopting fireproof coating. Studies in the field of fire design aim to break this paradigm and better understand the phenomena associated with the fire itself or the behavior of structures at high temperatures, thus allowing safer and more economical buildings.

In 1986 Robinson and Latham (1986 apud Wang [9]) point out that the use of fireproof coatings represented 30% of the total cost of a steel structure, which created a huge disadvantage in relation, mainly, to concrete structures. With this problem in mind, both the steel industry and the scientific community sought to study the effect of fire on structural elements.

The benefits of composite steel and concrete construction in fire resistance, when compared to an isolated steel structural element, have been the subject of studies by several authors. By comparing a composite steel and concrete beam numerical model to Cardington's tests results, Usmani et al. [10] highlight the importance of taking into account the thermal expansion coefficient of the materials so that the results are closer to reality. They also conclude that large deformations in the concrete slab induce a membrane behavior, which is responsible for preventing its collapse, thus

highlighting the importance of slab's mesh reinforcement to resist these stresses and significantly increasing the strength of composite elements.

Bailey et al. [11] investigated the effects of membrane stresses on the behavior of composite slabs in fire through laboratory tests. Subsequently Bailey [12] proposed a theoretical formulation capable of incorporating this effect in the evaluation of the structural collapse of the slab in fire. By numerical models, Lim et al. [13] conclude that for one-direction slabs, if the supports are able to restrain horizontal movements, large deformations allow the structure to behave similarly to a cable, resisting vertical actions by means of tensile stresses, featuring a catenary effect. Advanced numerical models benefit from this, as they incorporate geometric non-linearity. When considering the slab's semi-continuity, the mesh reinforcement at the supports is fundamental to resist these horizontal stresses, indicating that providing composite connections for floor beams can result in an increase in its strength in fire.

Through a series of laboratory tests, Anderson and Najafi [14] confirm that the mesh reinforcements in composite connections have a great influence on support's resilience and rotation capacity. They note that the composite connection capacity can be about 3 times greater than a simple steel connection and the mesh reinforcement ratio have a great influence in this behavior. These results indicate that investigating the influence of the mesh reinforcement in the behavior of composite beams in fire can considerably increase its strength.

Lin et al. [15] highlight the role of concrete slab mesh reinforcement to resist catenary stresses. By finite elements analysis they studied three different reinforcement meshes, noting that the effect of the reinforcement ratio becomes relevant after the unprotected beams reach a temperature of 500 °C, when the catenary effect is introduced by great deformations. The author concludes that the collapse behavior of the concrete slab in a fire is directly dependent on the configuration and strength of the reinforcement mesh.

Ioannides and Mehta [16], who adopted as design criteria the formation of plastic hinges in the mid-span and in the supports, have already proposed considering the semi-continuity of composite beams in a fire and stated, for protected beams, that there is a relevant increase in its bending moment strength. The authors also state that most of composite beams are designed at room temperature to meet deformation limits, thus having a reserve in their bending capacity for fire design, where service limit states are not considered.

Fakury et al. [17] compared simply supported and semi-continuous composite protected beams, using the design method proposed by Eurocode EN 1994-1-2 [18]. As a conclusion, they found out a strength increase of 116% to 123% for the semi-continuous protected composite beams when compared to the simply supported case.

Fischer and Varma [19] analyzed composite beam frames with typical hinged connections (shear plates, single angles and double angles) by three-dimensional finite elements numerical models. They compared simple frame models with multiple frames, taking into account the continuity of the slab through the floor, thus having a negative bending moment in the supports. As a conclusion, they state that the slab's continuity and the reinforcement mesh have a great influence on beam's and connection's structural behavior during fire, also stating that there was no premature failure of the connections during fire exposure.

Romagnoli and Silva [20] studied the behavior of unprotected composite beams in fire by taking into account the rotational stiffness in the supports provided by the slab's reinforcement mesh and restriction of the steel's profile lower flange, forming a composite connection. The calculations followed ABNT NBR 14323 [6] design procedures for standard-fire resistance requirements of 30 min. The authors evaluated that, although there is a significant increase of the semi-continuous beam bending strength compared to the simply supported case (about 90% increase), this procedure is not enough to dispense fireproof coatings. Subsequent studies [2] have shown that, in specific cases, it is possible to dispense fireproof coatings by following design codes procedures for standard-fire resistance requirements lower than 30 min.

1.3 Problem analysis

The numerical models were developed in ABAQUS software version 6.12-1 and represents a composite steel and concrete beam made of Gerdau brand steel profile and a 2 meters width solid concrete slab, that is, without steel sheeting, with shear connectors welded directly to the steel profile's upper flange. The slab has a steel reinforcement mesh made of steel bars located 3 cm away from the slab's upper face. The rebar longitudinal spacing varies from case to case for each model according to the calculated reinforcement ratio while the transversal spacing is 20 cm for all models.

Thermal loading is applied on the bottom face of the concrete slab and on all faces of the steel profile, excluding the steel's profile upper flange upper face, which is in direct contact with the concrete slab. The room's temperature starts at 20 °C and changes over time according to ISO 834 curve. The α_c convection heat transfer coefficient was

defined constant and equal to 25 W/(m².°C) and the emissivity equal to 0.7, as recommended by ABNT NBR 14323 [6] in order to follow the hypotheses adopted in the simplified method. Shading effects were not take into account.

To associate the composite connection bending strength only with the steel profile characteristics, bolts strength and sitting angle thickness were admitted compatible with the steel profile, thus, eliminating the need to evaluate various conditions. In other words the conditions presented in Equation 1, according to ABNT NBR 8800 [1], must be satisfied during the evaluation of the semi-continuous composite beam bending strength in fire.

$$n_b F_{b,Rd} \geq 1,25 f_{yd} A_{f,inf} \tag{1a}$$

$$F_{L,yd} A_L \geq 1,25 f_{yd} A_{f,inf} \tag{1b}$$

where: n_b is the number of bolts; $F_{b,Rd}$ is the bolt shear design strength; $F_{L,yd}$ is the lower angle yield design strength; $A_{f,inf}$ is the steel profile lower flange cross-sectional area; and A_L is the lower angle cross-sectional area.

2 NUMERICAL MODEL VALIDATION

For validation of finite elements techniques used, numerical models were developed prior to the study. The validation models' results were compared to the experimental results collected by Wainman and Kirby [21], who performed several tests in Swinden's laboratories in Rotterdam, England. They evaluated the behavior of composite beams subjected to high temperatures, registering the furnace, lower flange, web and upper flange temperatures and the vertical mid-span displacement of the beam over time. The tests chosen as a reference for validation will be the so-called test 15 and test 16. The choice for these tests is due to the fact they represent unprotected steel profiles, thus, being the closest to the subsequent models evaluated in the paper.

Both tests follow the configuration as seen by the longitudinal section in Figure 2. It represents a composite beam with a British steel profile UB 254x146x43 and a concrete slab 642 mm wide and 130 mm thick, two lines of 19 mm diameter shear connectors spaced 95 mm across and 280 mm longitudinally, providing composite interaction between the parts. The beam covers a 4530 mm span and the steel profile is supported on rollers that allow its ends to rotate and move. The concrete slab has a reinforcement mesh of 8 mm diameter steel bars spaced 200 mm apart and arranged 35 mm from the slab's bottom face. Four concentrated forces spaced 1133 mm and symmetrical in relation to the middle span are applied throughout the test. The steel profile is class BS 43A and the concrete has a compressive strength of 30 MPa.

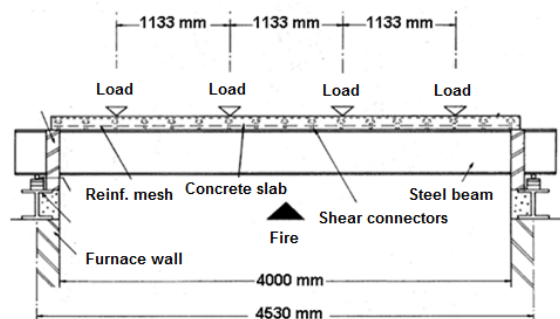


Figure 2. Test arrangement longitudinal section (Source: adapted from Wainman [21]).

The profile steel yield strength at room temperature was measured in laboratory, resulting in 280 MPa for test 15 and 273 MPa for test 16. Steel's ultimate strength resulted in 469 MPa for test 15 and 481 MPa for test 16 at an elongation of 25%.

Each of the four applied forces is equivalent to 32.47 kN for test 15 and 62.36 kN for test 16.

The furnace used in tests is gas powered and horizontal, 4 m long, 3 m wide and 1.8 m high. The furnace temperatures sought to follow the curve defined in BS 476: 1972 - part 8, which is similar to the ISO 834 curve.

The thermal analysis used three-dimensional prismatic elements with 20 node each, these located at the vertices and midpoint of the prism edges, called DC3D20 by Abaqus. Figure 3 illustrates the finite element mesh, its density was defined after analyzing several results of previous models.

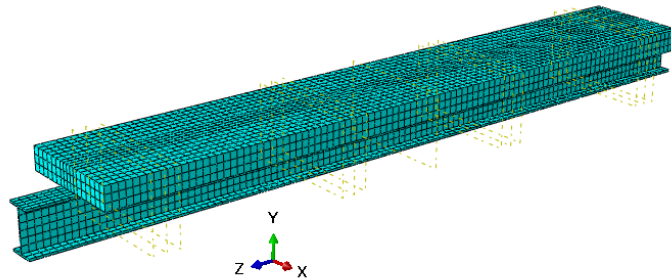


Figure 3. Finite element mesh.

The material’s thermal properties followed ABNT NBR 14323 [6] and ABNT NBR 15200 [5] recommendations. Stefan Boltzmann's constant was defined as $5.669 \times 10^{-8} \text{ W}/(\text{m}^2 \cdot ^\circ\text{C})$ and absolute zero temperature as $-273.15 \text{ }^\circ\text{C}$. Unlike ABNT NBR 14323 [6] recommendation of a constant emissivity of 0.7, the model followed the recommendations of Wong [22] and Cedeno et al. [23] that determine the furnace equivalent emissivity as dependent on the gases and structural element temperatures, according to Equation 2, simulating a more realistic condition.

$$\varepsilon_{eq} = \frac{\varepsilon_g T_g^4 - \alpha_g T_s^4}{T_g^4 - T_s^4} \tag{2}$$

where: α_g and ε_g are given by Equations 3 and 4.

$$\alpha_g = X_1 T_s^{X_2} + T_g^{X_3} \tag{3}$$

$$\varepsilon_g = X_4 + X_5 T_g \tag{4}$$

where: X_1 a X_5 coefficients (Table 1) were defined empirically by Wong [22] as a function of L_m length, given by Equation 5, and are related to the furnace length L , width w and height h .

$$L_m = \frac{1.8 h w}{h + w + \frac{h w}{L}} \tag{5}$$

Table 1. X_1 to X_5 coefficients.

L_m	X_1	X_2	X_3	X_4	X_5
0.5	6.432499	-1.02349	0.499770	0.302	-0.000118
1	4.249018	-0.91824	0.493256	0.373	-0.000135
2	2.578352	-0.77310	0.457589	0.443	-0.000140
3	1.845211	-0.68851	0.441610	0.479	-0.000133
4	1.448499	-0.63266	0.434033	0.501	-0.000124
5	1.202279	-0.59368	0.431480	0.517	-0.000115
6	1.036789	-0.56531	0.431575	0.527	-0.000106

Source: Wong [22].

Using the temperature field resulted by the thermal analysis, a structural analysis of the same finite element mesh was performed, but now with first order and reduced integration prismatic finite elements, called C3D8R by Abaqus. The steel's and concrete's mechanical properties reduction due to high temperatures followed ABNT NBR 14323 [6] and ABNT NBR 15200 [5] recommendations. Shear connectors and mesh rebars were modeled as Timoshenko beam elements, called B31 by Abaqus and embedded in the concrete slab as shown in Figure 4.

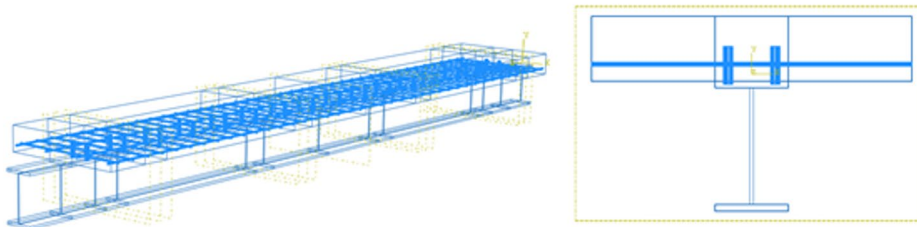


Figure 4. Slab embedded beam elements.

Steel's constitutive model was represented by the Classical Metal Plasticity model being applied to the steel profile, shear connectors and mesh reinforcement elements, with their stress values as function of deformation and temperature as seen in Figure 5. The concrete behavior was represented by the Concrete Damaged Plasticity, with input parameters according to Kmiecik and Kaminski [24] recommendations and temperature dependent mechanical properties as seen in Figure 6 and Figure 7.

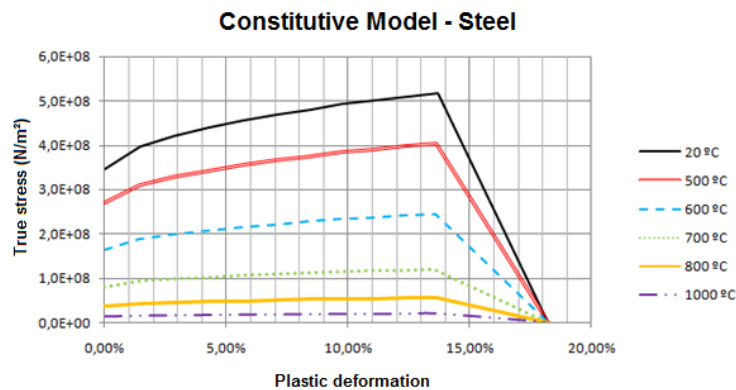


Figure 5. Steel mechanical properties.

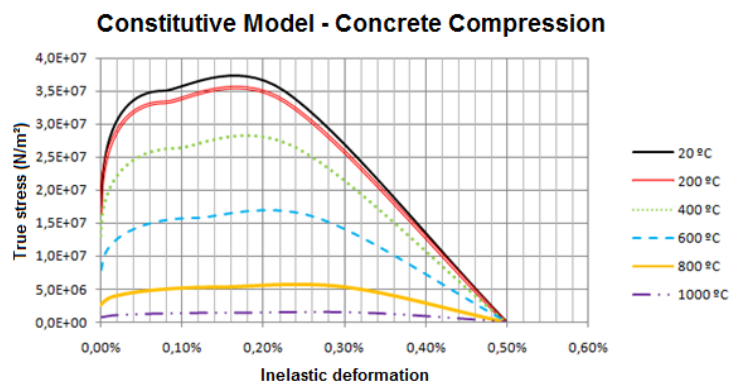


Figure 6. Concrete mechanical properties under compression.

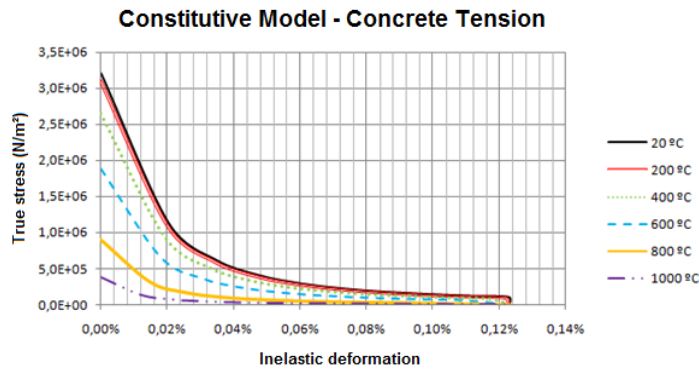


Figure 7. Concrete mechanical properties under tension.

The boundary conditions are such that they prevent the vertical and transverse displacement of the beam’s ends, while allowing its rotation and longitudinal movement. Figure 8 illustrates the web region in which all the nodes were prevented from moving along the Y axis. In addition to self-weight, applied as a gravitational field, each of the four concentrated forces reported in the tests was applied as a distributed load in the slab’s upper face in a rectangle area with one side equals to the steel profile flange width (also seen in Figure 8), in order to avoid stress concentration in a single mesh node.

The graphs in Figure 9, shows the lower flange, web and upper flange temperature resulted in the numerical thermal analysis and compared to Wainman and Kirby [21] records of test 15 and the mid-span vertical displacement over time.

Figure 10 graphs record lower flange, web and upper flange temperatures found in the numerical thermal analysis and compared to Wainman and Kirby [21] for test 16 and the vertical displacement in the middle of the span over time.

The results of both thermal and structural analysis showed good relations with laboratory tests, indicating that the materials properties, mesh density and finite element type, numerical precision, boundary conditions and other adopted parameters are acceptable to represent a real case scenario.

3 NUMERICAL MODELS

3.1 Geometry

Table 2 shows each numerical model geometric characteristics, being:

d the steel profile height; t_w the steel profile web thickness; b_f the steel profile flange width; t_f the steel profile flange thickness; t_c the concrete slab thickness; b the concrete slab effective width; ρ the maximum reinforcement ratio for the fire resistance time determined by the simplified method; \varnothing the rebar diameter; s the rebar spacing; L the beam span; n_{cs} the number of shear connectors required for full composite interaction at room temperature; M_{Rd}^+ the positive bending moment strength designed for room temperature; q the uniformly distributed load which results in a positive bending moment same as M_{Rd}^+ for the simply supported case; $0.7q$ 70% of q , representing a load reducing factor for fire design; “FRT simpl.” the Fire Resistance Time determined from the simplified method adopting a load factor of 0.7 for the same geometrical parameters.

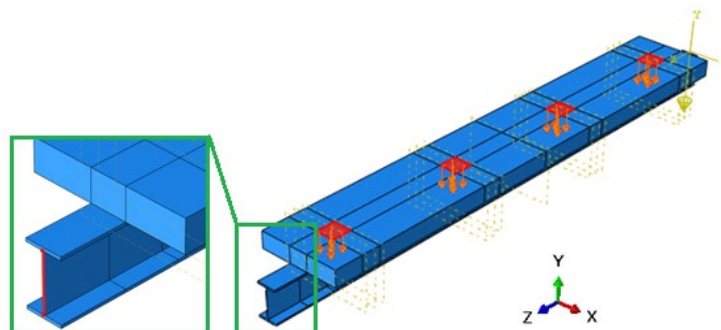


Figure 8. Load applied regions and Y axis restrained region.

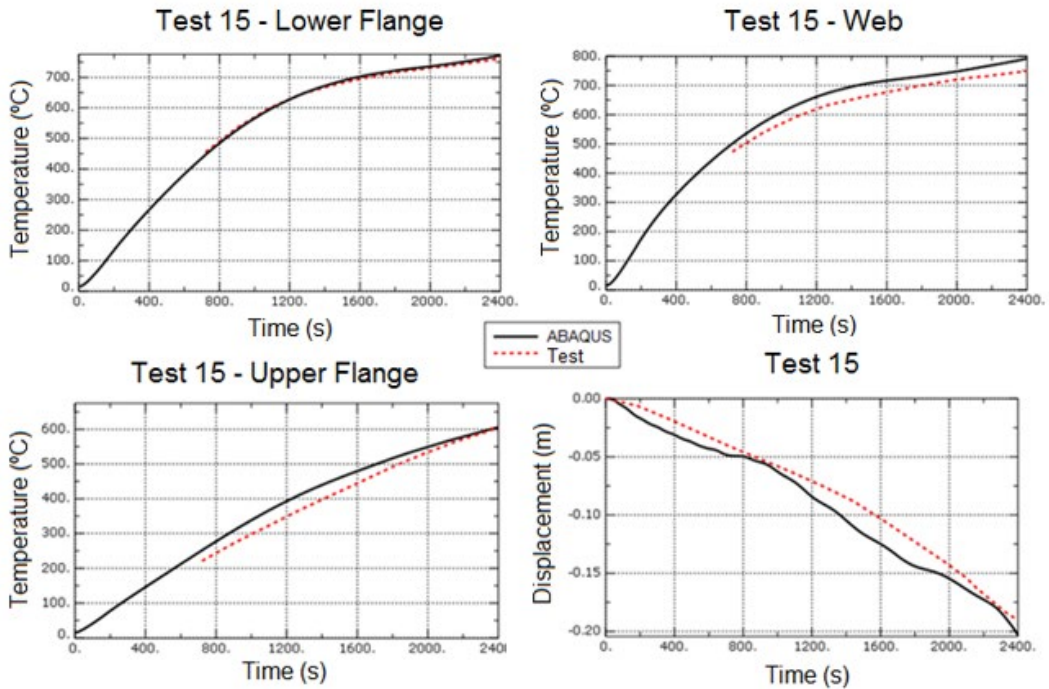


Figure 9. Numerical model compared to Test 15 results.

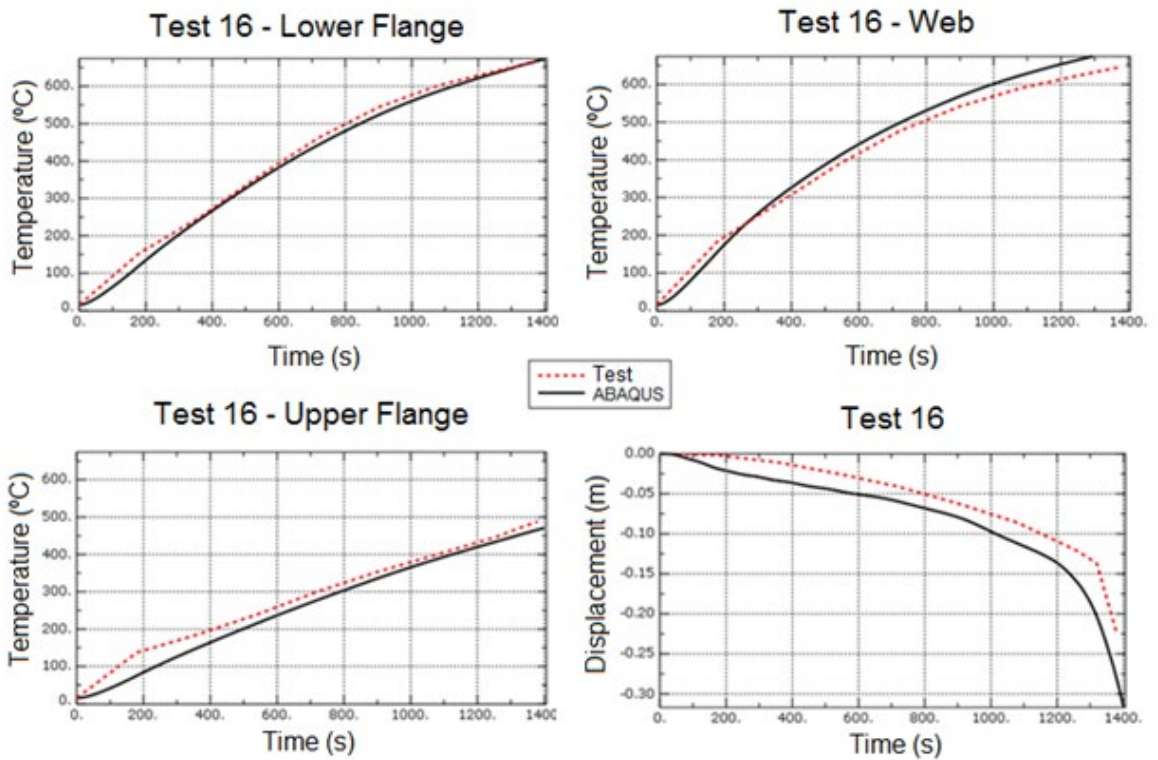


Figure 10. Numerical model compared to Test 16 results.

Table 2. Model parameters.

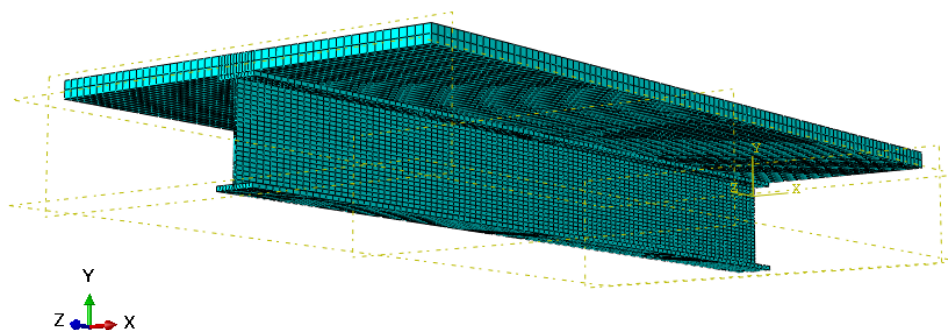
Profile	Model 1	Model 2	Model 3	Model 4	Model 5	Model 6	
	W250x25.3	W460x106.0	W530x85.0	W250x89.0	W360x51.0	W610x174.0	
d	257	469	535	260	355	616	mm
t_w	6.1	12.6	10.3	10.7	7.2	14.0	mm
b_f	102	194	166	256	171	325	mm
t_f	8.4	20.6	16.5	17.3	11.6	21.6	mm
Slab characteristics							
t_c	8	8	12	12	18	18	cm
b	200	200	200	200	200	200	cm
ρ	0.48	2.41	1.32	1.36	0.52	1.68	%
\emptyset	10	20	20	20	16	25	mm
s	10	8	10	9	10	8	cm
General parameters							
L	5.0	8.0	8.0	5.0	8.0	12.0	m
n_{cs}	20	60	68	72	40	132	un.
M_{Rd}^+	194.2	1094.1	1141.1	712.2	658.1	2720.7	kN.m
q	62.1	136.8	142.6	227.9	82.3	151.1	kN/m
$0.7q$	43.5	95.7	99.8	159.5	57.6	105.8	kN/m
FRT simpl.	<15	22	18	25	17	25	min.

Material's thermal and mechanical properties followed all ABNT NBR 14323 [6] and ABNT NBR 15200 [5] recommendations.

The steel class adopted is ASTM A572 Gr. 50 with 345 MPa yield strength and 450 MPa ultimate strength. The start elongation at yield was defined as 0.2% and at break as 15%. The reinforcement mesh was defined as steel class CA50 with 500 MPa yield strength. Shear connectors were modeled with a 450 MPa ultimate strength steel.

Concrete has a compressive strength of 30 MPa, tensile strength was defined following ABNT NBR 6118 [25] recommendations.

Finite element mesh has an average size of 5 cm, resulting in meshes with density similar to that used in the validation model, as shown in Figure 11. For the thermal analysis, DC3D20 elements were used, while for the structural analysis, steel profile and the concrete slab were modeled with C3D8R solid elements and shear connectors and mesh rebars with B31 beam elements.

**Figure 11.** Finite elements mesh density representation.

3.2 Boundary conditions

For each numerical model, three different boundary conditions were studied: axial released, axial restrained and semi-continuous. Table 3 summarizes the restrain conditions for each region of each element that form the composite beam (Figure 12), characterizing the boundary conditions mentioned.

Table 3. Boundary conditions.

Support Element	Condition		
	Axial Released	Axial Restrained	Semi-continuous
Slab + Reinf. Mesh	Free	Fully restrained (X,Y and Z)	Fully restrained (X,Y and Z)
Upper flange	Free	Free	Free
Web	Y Restrained	Fully restrained (X,Y and Z)	Fully restrained (X,Y and Z)
Lower flange	Free	Free	Fully restrained (X,Y and Z)

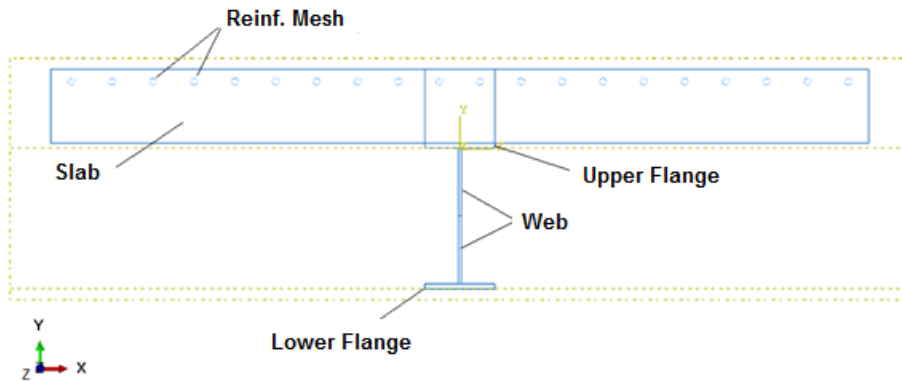


Figure 12. Support region sub-elements.

The axial released condition aims to assess the behavior of the beam in the hypothetical situation of a simplified analysis, where indirect axial forces resulting from thermal expansion or catenary effects due to large deformations do not contribute for the beam’s bending strength. Such a condition is hardly found in practice, especially in building floors, due to the complexity of the connection elements for releasing such movements.

The axial restrained condition evaluates a composite beam with its web restrained in the vertical and axial direction. The concrete slab is also restricted, simulating its continuity but with a minimum reinforcement ratio, made of 5 mm diameter rebars, commonly found in anti-cracking meshes. The idea here is to consider the most common conditions found in a floor beam, where there is only a connection between the profile’s web and the primary beam or column and minimum anti-cracking mesh. By comparing the results with the axial released condition, it is possible to assess whether the behavior of common constructive dispositions is close to the hypotheses considered in the simplified method.

The semi-continuous condition considers the restriction of the steel’s profile lower flange and increase of the concrete slab reinforcement mesh according to the simplified calculation as specified in Table 2, in addition to the restrictions of the axial restrained condition. By comparing the results to the axial restrained condition, it is possible to verify the effect of the lower flange restriction and increase of the slab’s reinforcement ratio on the composite beam behavior in fire.

The composite beams were loaded vertically on the slab’s upper face by a uniformly distributed load over the area equivalent to the beam’s entire length and width equal to the steel profile’s upper flange width b_f , as shown in Figure 13.

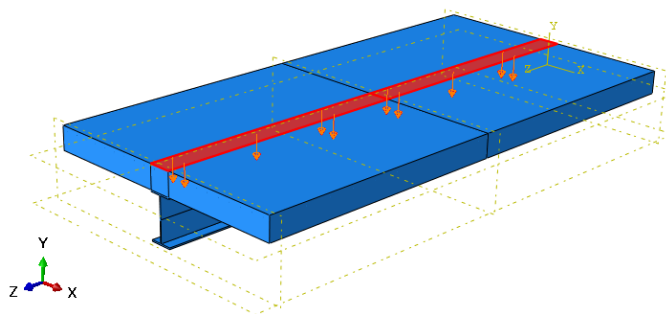


Figure 13. Distributed load application region.

The restraints represent perfect elastoplastic conditions, simulating a protected large beam or column as support for the composite beam. Besides the end supports, there are no transverse restrictions over the beam’s length.

A uniformly distributed horizontal load equivalent to 0.1% of the vertical load was applied to the steel profile’s lower flange to create an initial geometric imperfection and prevent numerical convergence for an unstable equilibrium. This load magnitude is sufficiently small to not interfere with the beam’s initial stress during the analysis.

4 RESULTS AND DISCUSSIONS

For the thermal analysis, Figure 14 graphs show the normalized temperature values, that is, for each coordinate the temperature value was divided by the square root of the sum of the squares of all values, standardizing the results and illustrating the temperature distribution along the height of the steel profile for each of the six models. The horizontal axis represents the distance from the lower flange to the upper flange, with zero being the steel profile’s lowest point.

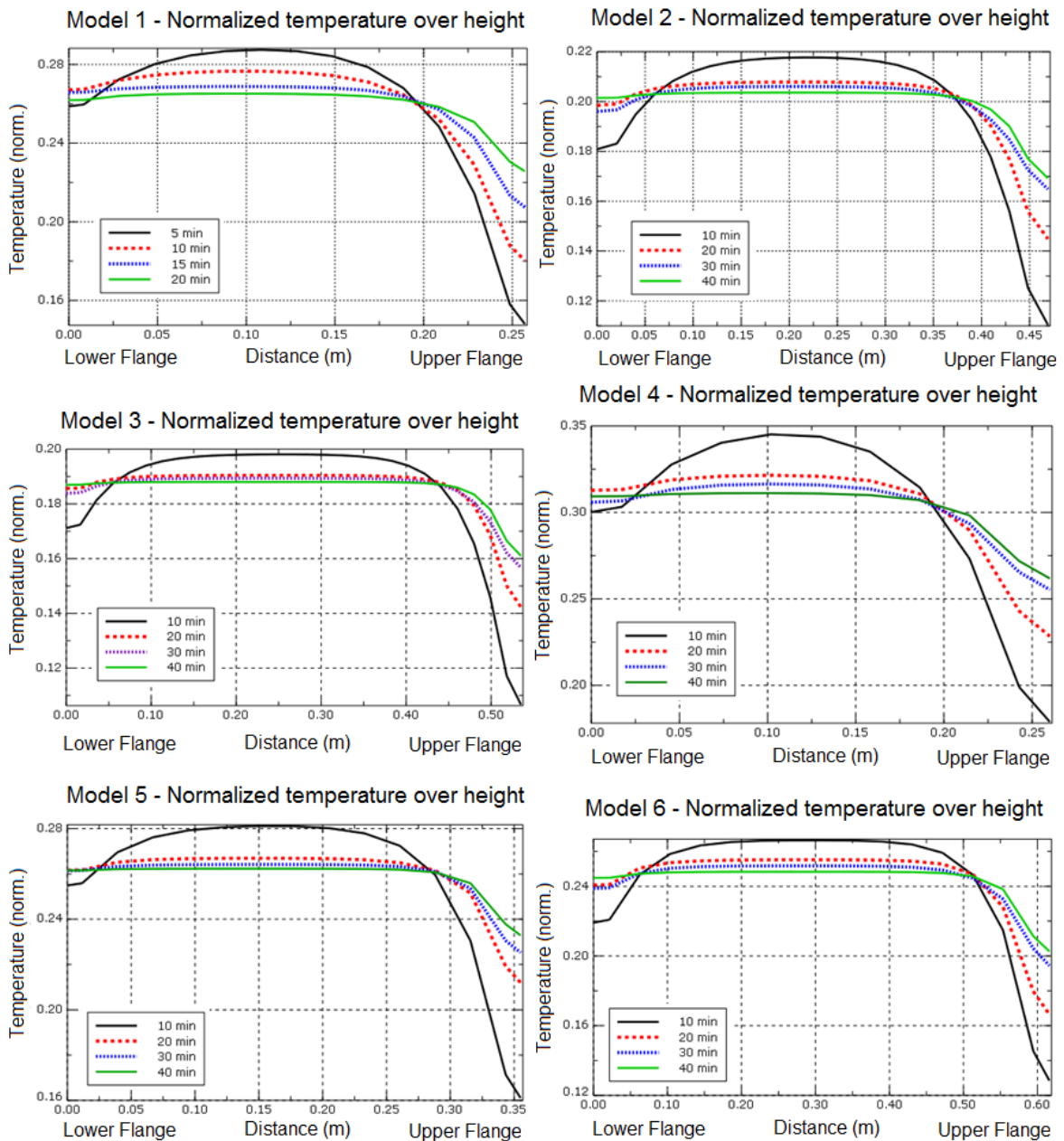


Figure 14. Normalized temperature over height.

It is noted in all models that the temperature distribution becomes uniform with the evolution of the standard fire, so that effects related to the thermal gradient are not evident for times greater than 15 min. The steel profile's lower flange and web have almost uniform temperatures, with a noticeable decrease only in the upper portion, equivalent to approximately 1/5 of the steel profile's total height, where it changes in a linear way up to the upper face.

For the structural analysis, graphs in Figure 15 show the mid-span vertical displacement, comparing the different boundary conditions proposed according to Table 3. Figure 16 illustrates the deformed model for the semi-continuous case at the exact moment when failure criteria was observed.

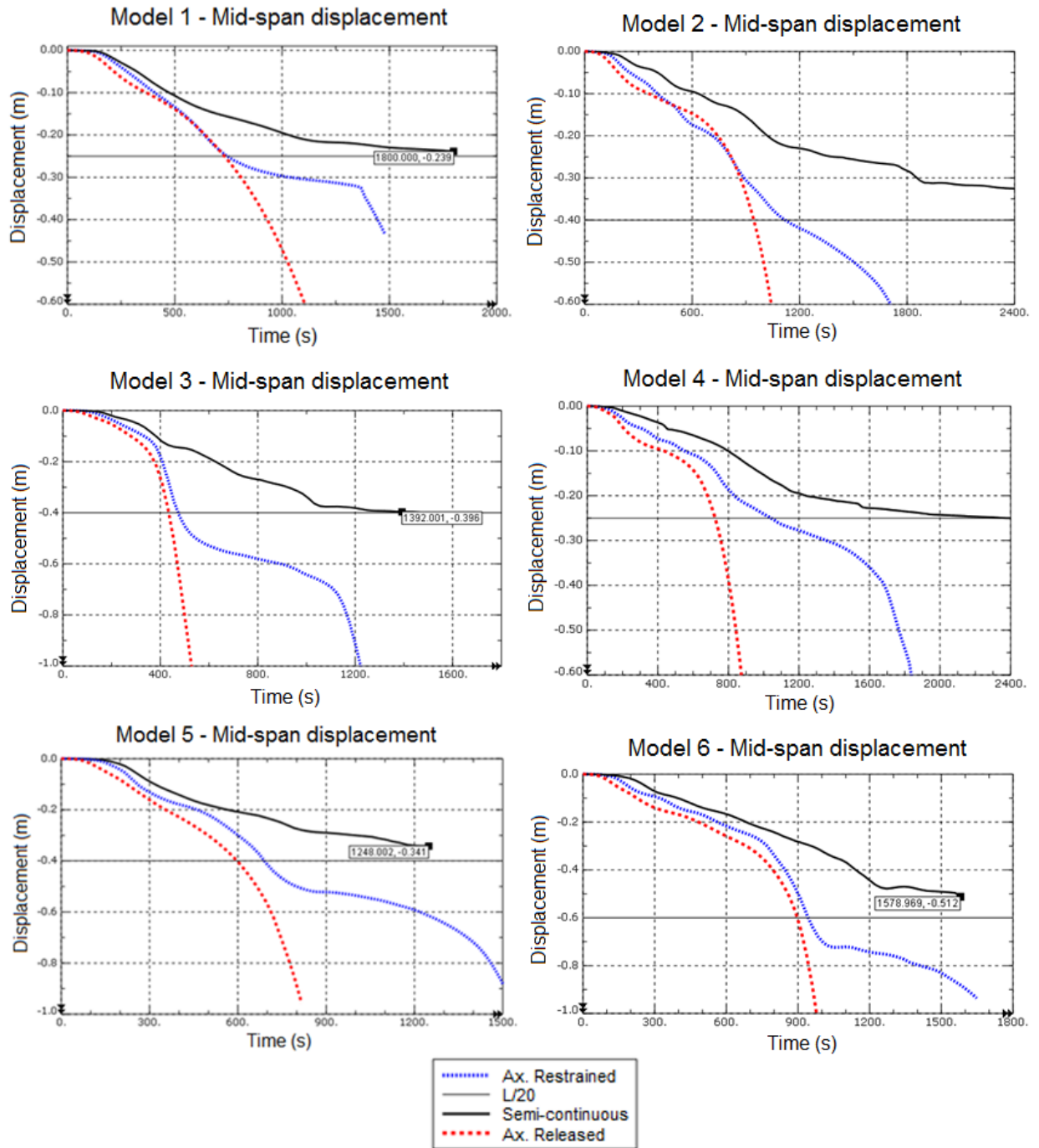


Figure 15. Mid-span displacement over time.

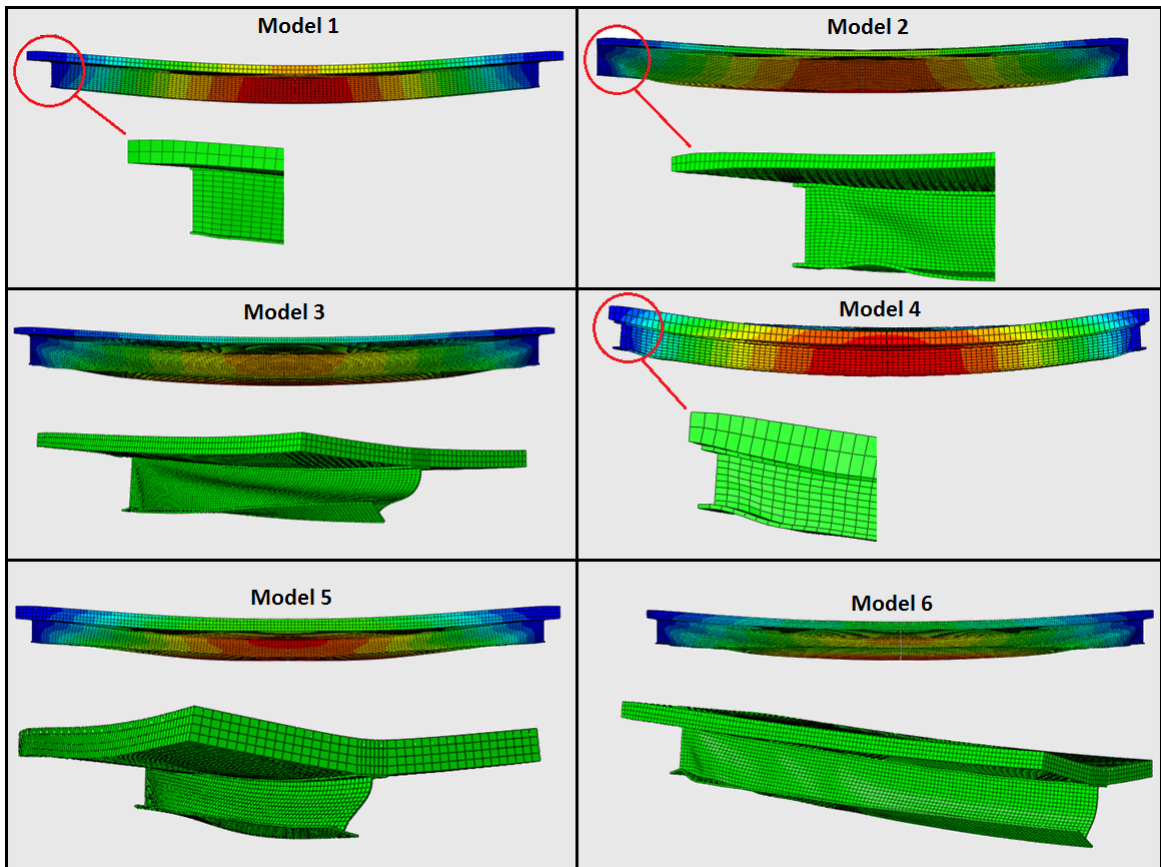


Figure 16. Deformation results for the semi-continuous case at collapse.

As a numerical nonlinear analysis is able to find equilibrium mechanisms usually overlooked in simplified analyzes, there is an intrinsic difficulty in characterizing structural collapse. Thus, following the same criteria as Wainman and Kirby [21] and Cedeno et al. [23], the collapse was defined according to BS 476 recommendations [26]. It is assumed that collapse is characterized as the first occurrence between (I) mid-span displacement greater than $L/20$ and (II) a displacement rate greater than $L^2/9000d$ after a displacement greater than $L/30$.

In addition, numerical non-convergence of the model, normally associated with excessively distorted elements, was considered a failure criterion, assuming that the beam no longer has the capacity to resist stresses properly.

For displacements below $L/20$ it can be noted that there is little difference between the axial released and axial restrained condition in all models, so that the hypothesis adopted in simplified methods, that is, neglecting axial indirect stress and the slab's continuity, are acceptable. For displacements greater than $L/20$, however, the displacement rate for the axial restrained case is notably lower when compared to the axial released case, so that collapse does not occur abruptly. For very high deformations, it is likely that large cracks will form on the slab, losing its fire sealing property, so it is important to follow the $L/20$ limit even if catastrophic failure does not occur.

In the semi-continuous condition, where the steel profile's lower flange was restrained and the slab's reinforcement ratio was considerably increased, the behavior of the composite beam changed dramatically, with an increase in its strength. The mid-span displacement rate was much lesser and catastrophic failure did not occur in any model, even after complete yield of the exposed steel profile.

Table 4 compares the fire resistance times (FRT) obtained in the numerical analysis for the semi-continuous case with values provided by the simplified method, in addition to indicating the failure criterion observed. Collapse condition (II) was not observed for the semi-continuous case, with numerical convergence and displacements greater than $L/20$ being the critical criteria for characterizing the composite beam collapse.

The numerical analysis predicted higher FRTs than the simplified method in all cases. The consideration of geometric and material nonlinearity allowed the concrete slab, provided with a reinforcement mesh, to resist vertical loads due to catenary effects. The large deformations, limited to $L/20$ as recommended by BS 476 [26], and being the

reinforced mesh protected from the temperature increase ensure that stresses are resisted in a behavior similar to a cable, a hypothesis already proven by several authors and ignored by the simplified method.

Table 4. Simplified method and numerical analysis FRTs comparison.

	FRT Simpl. Method	FRT Num. Analysis	Num. Analysis Fail Criteria
Model 1	< 15 min	30 min	$\delta = L/20$
Model 2	22 min	> 40 min	Not observed
Model 3	18 min	~23 min	$\delta = L/20$
Model 4	25 min	40 min	$\delta = L/20$
Model 5	17 min	~21 min	Numerical instability
Model 6	25 min	~26 min	Numerical instability

It is important to note that in order to take advantage of this phenomenon, it is necessary that the mesh reinforcement ratio is present in the entire length of the beam, and not only in negative bending moment region.

Another important aspect is the fact that the semi-continuous condition resulted in a large tensile area on the slab, especially in the region close to the supports. Such a region is highly subject to cracking. The proposed numerical models, however, are not able to assess the size of these cracks, so there is a possibility of loss of slab’s fire sealing property, allowing the heated gases to permeate the upper floor.

Models 3, 5 and 6 steel profiles suffered web distortion in the mid-span and local buckling in the support region, drastically reducing its strength in the first minutes (less than 15 min).

Such phenomenon, however, did not cause abrupt deformation of the composite beam. The mid-span displacement remained within the $L/20$ limit during fire, with the slab’s catenary effect being enough to resist the stresses and allowing equilibrium. Thus, even with the occurrence of web buckling, the numerical model FRT were superior to those found by the simplified method, where such effect was not considered. The occurrence of local instabilities caused greater deformations, which would be relevant for room temperature design where elastic behavior is sought through the building’s life span. For fire design, however, the local buckling was not enough to cause collapse or loss of fire sealing property within the time limits listed in Table 4.

It is important to note that the web distortion was not an exclusive phenomenon of the semi-continuous case, occurring for all boundary conditions in models 3, 5 and 6, including the axial released one, as illustrated by Figure 17.

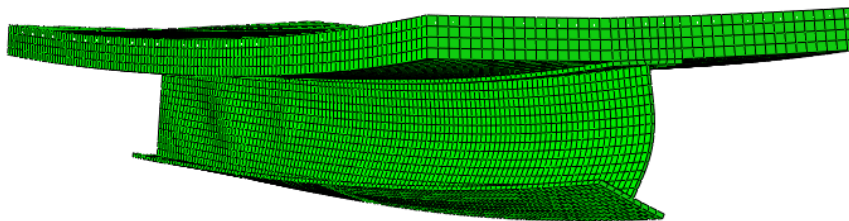


Figure 17. Web distortion detail for model 6, axial released case.

Despite being classified as a compact cross-section, large deformations induced web buckling as soon as the steel’s modulus of elasticity was reduced (temperatures above 300°C), since there is no presence of any intermediate stiffener or transverse bracing. Web stiffeners in mid-span allowing a connection between the lower and upper flanges could prevent this phenomenon.

Web distortion occurred for models with web slenderness greater than 40. It is suggested additional studies of this phenomenon for composite beams in fire.

5 CONCLUSIONS

Six unprotected composite steel and concrete beams numerical models were developed and submitted to a non-linear thermal and structural analyzes subjected to the standard fire while considering indirect stresses generated by

thermal expansion. For each model, three different boundary conditions were studied, namely: axial released, axial restrained and semi-continuous. The semi-continuous condition considers restriction of the steel profile lower flange and the continuity of the concrete slab over the end supports, with sufficient reinforcement mesh to develop the composite cross section maximum negative bending moment strength.

Structural analyses were performed for all conditions, and the results compared to FRT (Fire Resistance Time) values found by simplified analysis following design code procedures, where thermal expansion and geometric and material non-linearity effects are neglected.

By analyzing the results, it can be concluded that:

The temperature distribution along the steel profile's height becomes close to uniform with the standard fire evolution, so that effects associated with thermal gradient are reduced over time.

For a standard fire exposure greater than 15 min, the steel profile's temperature distribution along its height is close to uniform up to 1/5 of the upper portion, where it varies linearly to the upper face that is in direct contact with the slab.

For displacements below $L/20$ there is little difference between the axial released and axial restrained cases in all models, so that the hypotheses of neglecting the axial thermal expansion indirect stresses and the slab's continuity adopted in the simplified methods are acceptable. For displacements greater than $L/20$, however, the mid-span displacement rate of the axial restrained case is notably less pronounced compared to the axial released case, so that collapse does not occur abruptly.

If only the slab continuity over the supports are considered, by not increasing the reinforcement mesh and without restricting the profile's lower flange, there is no significant change in the composite beam FRTs compared to the axial released case, despite avoiding a catastrophic collapse. Since the axial restrained condition has resulted in higher FRTs than the axial released case, there is no need to consider the stress increase by thermal expansion and thermal gradient in simplified analysis.

The steel profile's lower flange restriction and an increase in the slab's reinforcement ratio, allowing the semi-continuous behavior of the composite beam, considerably increased FRTs for all analyzed models. Even after total yield of the steel profile, the beam maintained its equilibrium due to catenary forces presented on the slab caused by large deformations and horizontal restriction of the slab supports.

The results confirm the hypothesis of the simplified method adopted in [2] and [20]. All FRTs found in the numerical analysis for the semi-continuous cases were higher than those estimated by the simplified method. The hypothesis of neglecting indirect stresses caused by thermal expansion and thermal gradient are valid, since considering geometric and material non-linearity was sufficient to significantly reduce those effects. It is worth mentioning that the slab's reinforcement mesh must extend over the beam's entire length, and not only in the negative bending moments region to take advantage of such beneficial effects. Thus, slab's catenary effect is guaranteed, and it is possible to achieve an equilibrium mechanism even after complete yield of the steel profile.

The semi-continuous case resulted in a large tensile region on the slab, especially close to the end supports. It is expected that such region will be subject to cracking, however the model is not able to assess the size of these cracks, so that there is a possibility of loss of slab's fire sealing property, allowing the heated gases to permeate the upper floor. The conclusions presented in this paper are valid only if vertical fire compartmentation is not a design requirement, a usual practice for small buildings that allow for standard fire resistance requirement times less than 30 minutes. It is recommended that future studies evaluate the size of these cracks and the potential loss of the slab's fire sealing property.

Web distortion in the mid-span occurred for steel profiles with web slenderness greater than 40, even in the axial released case (indicating that it was not caused due to restriction of the profile's lower flange), which resulted in much lower FRTs compared to models where it did not occur. Further studies are suggested to investigate this phenomenon for unprotected composite beams in fire with long unbraced lengths. Even with the occurrence of web buckling, fire resistance times for the semi-continuous case were higher than those estimated by the simplified method, where no buckling was considered.

ACKNOWLEDGMENTS

Grant 2018/14735-6, São Paulo Research Foundation (FAPESP) and Conselho Nacional de Pesquisa e Desenvolvimento Científico (CNPq).

REFERENCES

- [1] Associação Brasileira de Normas Técnicas, *Projeto de Estruturas de Aço e de Estruturas Mistas de Aço e Concreto de Edifícios*, NBR 8800, 2008.
- [2] L. C. Romagnoli and V. P. Silva, "About the consideration of semi-continuity in simply supported composite steel and concrete beams, to remove fireproof coatings for less than 30 minutes standard-fire resistance time," *Rev. IBRACON Estrut. Mater.*, vol. 12, pp. 1183–1204, 2019, <http://dx.doi.org/10.1590/s1983-41952019000500011>.
- [3] V. P. Silva, *Estruturas de Aço em Situação de Incêndio*, São Paulo: Zigurate, 2001.
- [4] São Paulo. Polícia Militar. Corpo de Bombeiros, "Instrução técnica nº 08: resistência ao fogo dos elementos de construção," DO, 2011.
- [5] Associação Brasileira de Normas Técnicas, *Projeto de Estruturas de Concreto em Situação de Incêndio*, NBR 15200, 2012.
- [6] Associação Brasileira de Normas Técnicas, *Projeto de Estruturas de Aço e de Estruturas Mistas de Aço e Concreto de Edifícios em Situação de Incêndio*, NBR 14323, 2013.
- [7] V. P. Silva, C. N. Costa, and A. Melão, "Procedure for decreasing the required time for fire resistance of the multistory buildings," *Rev. IBRACON Estrut. Mater.*, vol. 10, no. 5, pp. 1141–1162, 2017., <http://dx.doi.org/10.1590/s1983-41952017000500011>.
- [8] L. C. Romagnoli "Análise de vigas mistas de aço e concreto semicontínuas em situação de incêndio," M.S. thesis, Dep. Eng. Estr. Geotéc., Esc. Politéc., Univ. São Paulo, São Paulo, 2018.
- [9] Y. C. Wang, *Steel and Composite Structures – Behavior and Design for Fire Safety*. London: Spon Press, 2002.
- [10] A. S. Usmani, J. M. Rotter, S. Lamont, A. M. Sanad, and M. Gillie, "Fundamental principles of structural behavior under thermal effects," *Fire Saf. J.*, vol. 36, no. 8, pp. 721–744, 2001, [http://dx.doi.org/10.1016/S0379-7112\(01\)00037-6](http://dx.doi.org/10.1016/S0379-7112(01)00037-6).
- [11] C. G. Bailey, D. S. White, and D. B. Moore, "The tensile membrane action of unrestrained composite slabs simulated under fire conditions," *Eng. Struct.*, vol. 22, no. 12, pp. 1583–1595, 2001, [http://dx.doi.org/10.1016/S0141-0296\(99\)00110-8](http://dx.doi.org/10.1016/S0141-0296(99)00110-8).
- [12] C. G. Bailey, "Membrane action of unrestrained lightly reinforced concrete slabs at large displacements," *Eng. Struct.*, vol. 23, no. 5, pp. 470–483, 2000., [http://dx.doi.org/10.1016/S0141-0296\(00\)00064-X](http://dx.doi.org/10.1016/S0141-0296(00)00064-X).
- [13] L. Lim, A. H. Buchanan, and P. J. Moss, "Restraint of fire-exposed concrete floor systems," *Fire Mater.*, vol. 28, no. 24, pp. 95–125, 2004., <http://dx.doi.org/10.1002/fam.854>.
- [14] D. Anderson and A. A. Najafi, "Performance of composite connections: major axis end plate joints," *J. Construct. Steel Res.*, vol. 31, no. 1, pp. 31–57, 1994, [http://dx.doi.org/10.1016/0143-974X\(94\)90022-1](http://dx.doi.org/10.1016/0143-974X(94)90022-1).
- [15] S. Lin, Z. Huang, and M. Fan, "The effects of protected beams and their connections on the fire resistance of composite buildings," *Fire Saf. J.*, vol. 78, pp. 31–43, 2015, <http://dx.doi.org/10.1016/j.firesaf.2015.08.003>.
- [16] S. A. Ioannides and S. Mehta, *Restrained Versus Unrestrained Fire Ratings for Steel Structures – a Practical Approach*. Chicago, USA: Modern Steel Construction, 1997.
- [17] R. H. Fakury, E. B. Casas, F. F. Pacifico, and L. M. P. Abreu, "Design of semi-continuous composite steel-concrete beams at the fire limit state," *J. Construct. Steel Res.*, vol. 61, no. 8, pp. 1094–1107, 2005., <http://dx.doi.org/10.1016/j.jcsr.2005.02.003>.
- [18] European Committee for Standardization, *Design of Composite Steel and Concrete Structures – Part 1-2 – General Rules – Structural Fire Design*, EN 1994-1-2: Eurocode 4, 2005.
- [19] E. C. Fischer and A. H. Varma, "Fire resilience of composite beams with simple connections: parametric studies and design," *J. Construct. Steel Res.*, vol. 128, pp. 119–135, 2017., <http://dx.doi.org/10.1016/j.jcsr.2016.08.004>.
- [20] L. C. Romagnoli and V. P. Silva, "About the use of semi-continuity to remove fireproof coatings in simply supported composite steel and concrete beams," *Rev. IBRACON Estrut. Mater.*, vol. 11, no. 2, pp. 296–306, 2018., <http://dx.doi.org/10.1590/s1983-41952018000200005>.
- [21] D. E. Wainman and B. R. Kirby, *Compendium of UK Standard Fire Test Data – Unprotected Structural Steel – 1*. Rotherham: BSC, 1987.
- [22] M. B. Wong, "Effect on temperatures of structural steel in fire," *J. Struct. Eng.*, vol. 131, no. 1, pp. 16–20, 2005., [http://dx.doi.org/10.1061/\(ASCE\)0733-9445\(2005\)131:1\(16\)](http://dx.doi.org/10.1061/(ASCE)0733-9445(2005)131:1(16)).
- [23] G. A. Cedeno, A. H. Varma, and J. Gore, "Predicting the standard fire behavior of composite steel beams," *Compos. Constr. Steel Concr.*, vol. 6, pp. 642–656, 2011., [http://dx.doi.org/10.1061/41142\(396\)53](http://dx.doi.org/10.1061/41142(396)53).
- [24] P. Kmiecik and M. Kaminski, "Modelling of reinforced concrete structures and composite structures with concrete strength degradation taken into consideration," *Arch. Civ. Mech. Eng.*, vol. 11, no. 3, pp. 623–636, 2011., [http://dx.doi.org/10.1016/S1644-9665\(12\)60105-8](http://dx.doi.org/10.1016/S1644-9665(12)60105-8).
- [25] Associação Brasileira de Normas Técnicas, *Projeto de Estruturas de Concreto – Procedimento*, NBR 6118, 2014.
- [26] Comité Européen de Normalisation, *Fire Tests on Building Materials and Structures – Part 20: Method for Determination of the Fire Resistance of Elements of Construction (General Principles)*, BS 476, 1987.

Author contributions: VPS: conceptualization, methodology, supervision; LCR: data curation, methodology, writing, formal analysis.

Editors: José Marcio Calixto, José Luiz Antunes de Oliveira e Sousa, Guilherme Aris Parsekian.